Strain relaxation mechanisms of elastic softening and twin wall freezing associated with structural phase transitions in $(Ca,Sr)TiO_3$ perovskites

2014 J. Phys.: Condens. Matter 26 505402

(http://iopscience.iop.org/0953-8984/26/50/505402)

OPEN ACCESS
IOP Publishing
Journal of Physics: Condensed Matter
J. Phys.: Condens. Matter **26** (2014) 505402 (14pp)
doi:10.1088/0953-8984/26/50/505402

Strain relaxation mechanisms of elastic softening and twin wall freezing associated with structural phase transitions in $(Ca,Sr)TiO_3$ perovskites

N J Perks[1], Z Zhang[2,3], R J Harrison[2] and M A Carpenter[2]

[1] Clarendon Laboratory, Department of Physics, University of Oxford, Parks Road, Oxford OX1 3PU, UK
[2] Department of Earth Sciences, University of Cambridge, Downing Street, Cambridge CB2 3EQ, UK
[3] Department of Metallic Materials, School of Materials Science and Engineering, Wuhan University of Technology, 122 Luoshi Road, Wuhan, 430070 China

E-mail: mc43@esc.cam.ac.uk

Received 28 July 2014, revised 23 September 2014
Accepted for publication 1 October 2014
Published 24 November 2014

Abstract

Resonant ultrasound spectroscopy has been used to measure the bulk modulus (K), shear modulus (G) and acoustic dissipation of polycrystalline perovskite samples across the $CaTiO_3$–$SrTiO_3$ solid solution in the temperature range ~10–1350 K. A remarkable pattern of up to ~25% softening of G as a function of both temperature and composition is due to coupling of shear strain with order parameters for the $Pm\bar{3}m \leftrightarrow I4/mcm$, $I4/mcm \leftrightarrow Pnma$ and $I4/mcm \leftrightarrow Pbcm$ transitions. Anomalies in K associated with the phase transitions are small, consistent with only weak coupling of octahedral tilting order parameter(s) with volume strain. A change from tricritical character for the $Pm\bar{3}m \leftrightarrow I4/mcm$ transition towards second order character at Sr-rich compositions appears to be due to changing properties of the soft optic mode rather than to changes in magnitude of strain/order parameter coupling coefficients. Precursor softening of G ahead of the $Pm\bar{3}m \leftrightarrow I4/mcm$ transition, due to fluctuations or clustering, occurs over a temperature interval of up to ~200 K, and also changes character at the most Sr-rich compositions. The tetragonal structure with Sr-rich compositions is characterized by additional softening with falling temperature which is most likely related to the proximity of a ferroelectric instability. The $I4/mcm \leftrightarrow Pnma$ transition is accompanied by stiffening, which is attributed to the effects of strong coupling between order parameters for M-point and R-point tilting. The pattern of attenuation at RUS frequencies in the tetragonal phase can be understood in terms of the mobility of twin walls which become pinned below ~500 K, and the loss mechanism most likely involves local bowing of the walls by lateral motion of ledges rather than the advance and retraction of needle tips. Twin wall mobility is suppressed in the orthorhombic structure.

Keywords: phase transitions, elasticity, acoustic dissipation

(Some figures may appear in colour only in the online journal)

1. Introduction

The ideal composition of the natural mineral perovskite (named originally after Count Perovskii) is $CaTiO_3$. It undergoes octahedral tilting transitions at ~1500 and

~1635 K, which combine as the classical M- and R-point tilt instabilities to give the characteristic structure with space group *Pnma*. $SrTiO_3$ (which also occurs as a natural mineral, tausonite) has a single R-point tilting transition at 106 K to give one of the next most common perovskite structures with space group $I4/mcm$. Both have been intensively studied as exemplars of phase transitions driven by soft optic modes (e.g. Unoki and Sakudo 1967, Shirane and Yamada 1969, Cowley *et al* 1969, Worlock *et al* 1969, Müller and Berlinger 1971, Redfern 1996, Kennedy *et al* 1999, Ali and Yashima 2005, and many subsequent papers), but also as end-members of a solid solution which displays analogue structure–property relationships for comparison with (Mg,Fe)SiO_3 perovskite in the Earth's lower mantle (Webb *et al* 1999, Qin *et al* 2000, 2002, Carpenter *et al* 2001, 2007, Harrison *et al* 2003, Carpenter 2006a, 2007a, 2007b, Walsh *et al* 2008). $CaTiO_3$ has also been considered as a potential host phase to immobilize radioactive waste elements (Ringwood *et al* 1988).

It might have been anticipated that the $CaTiO_3$–$SrTiO_3$ (CST) solid solution would consist simply of separate stability fields for the parent cubic ($Pm\bar{3}m$) structure and the two different tilted structures, with transition temperatures for $Pm\bar{3}m \leftrightarrow I4/mcm$ and $I4/mcm \leftrightarrow Pnma$ transitions which vary more or less linearly with composition. It turns out that the phase diagram is phenomenologically much richer than this, however, as shown in figure 1 from Carpenter *et al* (2006b). Substituting the smaller cation Sr^{2+}, for Ca^{2+} in $CaTiO_3$ produces the expected approximately linear reduction in transition temperatures, but two additional structure-types appear at Sr-rich compositions. One involves a different system of tilts, which gives space group *Pbcm* and is associated with the irreducible representation T_4 at the $\alpha = 1/4$ point on the T line ($k = 1/2, 1/2, \alpha$) of the Brillouin zone (Ranjan *et al* 2000, 2001, Mishra *et al* 2002, 2006, Howard *et al* 2008, Carpenter *et al* 2006b). The second, shown tentatively as having point group *mm*2, is indicative of the fact that $SrTiO_3$ at ambient conditions is close to a ferroelectric instability which can be induced at low temperatures by a small amount of doping with Ca (Mitsui and Westphal 1961, Bednorz and Müller 1984, Bianchi *et al* 1994a, 1994b, 1995, Kleemann *et al* 1995, 1997) or by replacing ^{16}O with ^{18}O (Itoh *et al* 1999, 2004, Itoh and Wang 2000, 2003). The existence of multiple instabilities has given the CST system an additional interest in the context of multifunctional materials whose properties depend directly or indirectly on combinations of ferroic phase transitions. A common theme in this much broader context has been the role of strain in relation both to the mechanisms by which multiple order parameters interact and by which otherwise mobile transformation microstructures become pinned.

The purpose of the present study was to investigate acoustic properties across the CST solid solution using resonant ultrasound spectroscopy (RUS), with a specific focus on the effect of composition on strain relaxation accompanying ferroelastic (tilting) and ferroelectric transitions, pinning of ferroelastic twin walls in the different structure types and the influence of fluctuations ahead of the different phase transitions. The particular advantage of RUS here is that

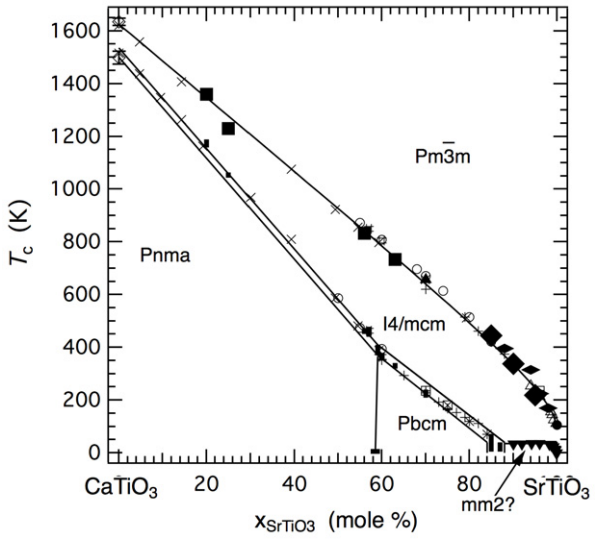

Figure 1. Subsolidus phase diagram for CST perovskites following Carpenter *et al* (2006b) based on data for transition temperatures from the literature. Parallel lines are estimates for the boundaries of the two-phase field between tetragonal and orthorhombic phases. The curved line is a fit to data for the transition temperature, T_c, of the cubic ↔ tetragonal transition.

data relating to elastic and anelastic properties can be obtained simultaneously over a wide temperature interval from samples with dimensions of a few mm (Migliori and Sarrao 1997), and that dense polycrystalline pellets of homogeneous CST perovskites with different compositions are reasonably easy to produce. Characteristic frequencies for mechanical resonances of such samples typically fall in the range ~0.1–3 MHz, which provides a valuable contrast with related elasticity and anelasticity data obtained by dynamical mechanical analysis (DMA) at ~0.01–100 Hz (Harrison *et al* 2003, Daraktchiev *et al* 2006) and pulse-echo ultrasonics at ~10–100 MHz (Carpenter *et al* 2007). Following the initial RUS study of Walsh *et al* (2008), use is made of the polycrystalline samples to map out variations of the bulk modulus, K, the shear modulus, G, and mechanical quality factor, Q, systematically as functions of temperature and composition.

2. Expected patterns of elastic softening and acoustic loss

Variations of elastic moduli due to phase transitions arise as a consequence of coupling between the macroscopic order parameter and strain and of acoustic modes with more local variations in structure. Small strains, typically of a few ‰ to a few %, can give rise to changes in individual elastic moduli of tens of % because they depend on the order parameter susceptibility. Quantitative descriptions of the elastic softening and stiffening associated with the $Pm\bar{3}m \leftrightarrow I4/mcm$ transition (R-point tilting) in $SrTiO_3$ were originally obtained by calibrating the coefficients in a standard 24 (second order) Landau free energy expansion (Lauberau and Zurek 1970, Slonczewski and Thomas 1970, Rehwald 1970a, 1970b, Lüthi and Moran 1970, Fossheim and Berre 1972, Okai

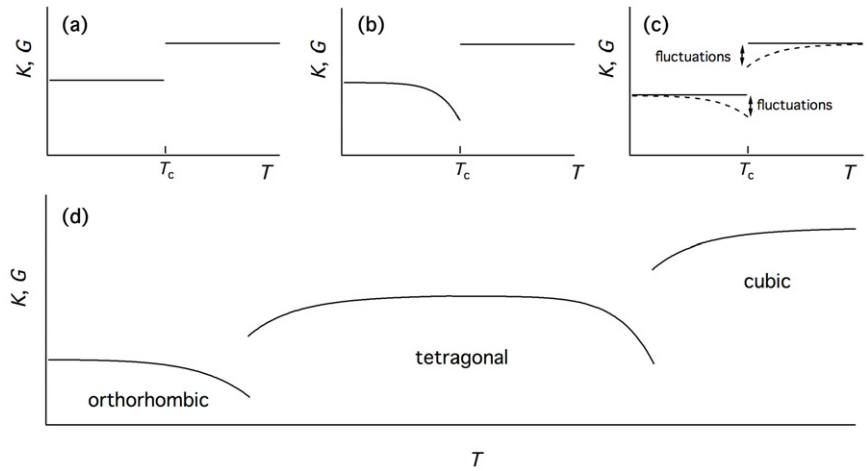

Figure 2. Schematic forms of expected variations of the bulk, K, and shear, G, moduli associated with tilting transitions in CST perovskites. (*a*) Second order transition. (*b*) Tricritical transition. (*c*) Second order with contributions from fluctuations, clustering, coupling of acoustic modes, etc. (*d*) Expected pattern for a cubic–tetragonal–orthorhombic sequence, including the influence of fluctuations/clustering but excluding anelastic effects relating to twin wall mobility under externally applied stress.

and Yoshimoto 1975). Following Salje *et al* (1998) and Hayward *et al* (1999), a 246 potential was found to provide a more complete description (Carpenter 2007a, 2009), and the transition changes towards tricritical character (26 potential) as the solid solution tends towards $CaTiO_3$ (Carpenter *et al* 2001, Carpenter 2007b). The simplest patterns of softening for the bulk and shear moduli expected on this basis are shown schematically in figure 2(*a*) (second order) and figure 2(*b*) (tricritical). *Pnma* is not a subgroup of *I*4/*mcm* so the same principles do not apply to the *I*4/*mcm* ↔ *Pnma* transition, but the expected pattern of elastic softening would not be grossly different from that expected for the $Pm\bar{3}m$ ↔ *I*4/*mcm* transition (Carpenter 2007a, 2007b, Carpenter *et al* 2007) since it depends primarily on the development of an M-point tilt, which also couples with strain. In $SrZrO_3$ the M-point tilting transition occurs as *Imma* ↔ *Pnma* and is close to being tricritical in character (Howard *et al* 2000), but in CST this is metastable and probably located within the stability field of the *I*4/*mcm* structure.

Elastic softening additional to the effects of classical strain/order parameter coupling is indicative of the influence of fluctuations, clustering, mobile microstructures and other dynamical effects such as central peak modes (figure 2(*c*)). In the case of transitions driven by a soft mode, the effects of fluctuations above the transition temperature can be understood in terms of contributions of the optic branch just away from the critical point (Pytte 1970, 1971, Axe and Shirane 1970, Höchli 1972, Rehwald 1973, Cummins 1979, Lüthi and Rehwald 1981, Yao *et al* 1981, Fossum 1985, Carpenter and Salje 1998). In the classic case of the $\alpha \leftrightarrow \beta$ transition in quartz, this premonitory softening conforms to a power law dependence on temperature and occurs over a temperature interval of at least ∼250 K in the bulk modulus but is barely detectable in the shear modulus (Carpenter *et al* 1998, Carpenter 2006, McKnight *et al* 2008). In ferroelectric and relaxor perovskites, it is observed in shear elastic constants over temperature intervals of ∼200–300 K (e.g. $BaTiO_3$, Ko *et al* 2008, Salje *et al* 2013a; $PbMn_{1/3}Nb_{2/3}O_3$, Carpenter *et al* 2012a; $PbZn_{1/3}Nb_{2/3}O_3$–$PbTiO_3$, Ko *et al* 2006, 2008, Farnsworth *et al* 2011; $PbIn_{1/2}Nb_{1/2}O_3$–$PbMn_{1/3}Nb_{2/3}O_3$–$PbTiO_3$, Nataf *et al* 2013, Kim *et al* 2012; $PbSc_{1/2}Ta_{1/2}O_3$, Aktas *et al* 2013). At least for $Pb(Mn_{1/3}Nb_{2/3})O_3$, the extent of softening of the shear modulus is comparable with that of the bulk modulus and perhaps conforms to a pattern of Vogel–Fulcher freezing behaviour (Carpenter *et al* 2012a). For tilting transitions in perovskites, the typical precursor interval for softening of the shear modulus in the stability field of the parent cubic structure is less than ∼50 K, however (e.g. $KMnF_3$, Carpenter *et al* 2012b; $SrTiO_3$; Carpenter 2007a; $SrZrO_3$ McKnight *et al* 2009a; $BaCeO_3$ Zhang *et al* 2010a; $LaAlO_3$ Carpenter *et al* 2010a). The key point is that these precursor effects provide evidence of local dynamic or static changes in structure which are additional to those expected from the normal mechanism of strain/order parameter coupling. The timescale of these types of fluctuations is short and generally does not lead to anelastic loss at RUS frequencies (∼0.1–1 MHz).

Fluctuations in local structure may also occur within the stability field of the low symmetry phase below the transition point, and one expression of this can be the development of central peak modes detected by Brillouin and Raman spectroscopy. A specific case is below the cubic ↔ rhombohedral transition in $LaAlO_3$ where the central peak mode(s) has been interpreted in terms of phonon density fluctuations and flipping of clusters of tilted octahedra between different orientations (Carpenter *et al* 2010b). These couple with the acoustic modes to produce softening in a temperature interval of up to ∼100 K below T_c which is superimposed on the normal effects of strain/order parameter coupling described by Landau theory. If such additional intrinsic softening mechanisms below and above the transitions points of CST perovskites are included, the full pattern for a sequence $Pm\bar{3}m$ ↔ *I*4/*mcm* ↔ *Pnma* might be expected to have the form shown in figure 2(*d*). At least for $LaAlO_3$, the relaxation time for the central peak mode(s) is ∼10–100 ps (Carpenter *et al* 2010b) and is therefore too short to be likely to give

rise to overt anelastic softening at the measuring frequencies of RUS.

The most characteristic cause of anelastic softening and dissipation associated with phase transitions is the mobility under external stress of ferroelastic twin walls. An applied stress induces a small strain according to Hooke's law in the normal way but, for appropriate orientations, a much larger strain can arise due to movement of the twin walls. Softening of specific shear moduli by tens of % due to this mechanism ('superelasticity'), together with strong attenuation, has been observed in $SrTiO_3$ and $LaAlO_3$, for example, and is due largely to the back and forth motion of the tips of needle twins (Schranz *et al* 1999, Kityk *et al* 2000a, 2000b, Harrison and Redfern 2002, Harrison *et al* 2004a, 2004b, Daraktchiev *et al* 2007, Carpenter and Zhang 2011). A temperature- and frequency-dependence characteristic of thermally activated mechanisms is observed for the acoustic loss because the twin wall motion is subject to viscous drag and eventual pinning by interaction with defects. The temperature interval of freezing or pinning where the walls become immobile is marked by a Debye peak in the dissipation. In the case of CST perovskites, twin wall mobility has already been shown to lead to a reduction of the Young's modulus of polycrystalline samples by up to 30% at frequencies of 0.01–50 Hz and the freezing interval in this frequency range is near 410 K (Harrison *et al* 2003, Daraktchiev *et al* 2006). Walsh *et al* (2008) and Carpenter and Zhang (2011) reported that resonance peaks disappeared entirely ('superattenuation') from RUS spectra collected from a sample of $Ca_{0.5}Sr_{0.5}TiO_3$ held in the stability field of the tetragonal structure (~600–940 K). At the relatively low stress and high frequencies of RUS measurements, in comparison with DMA measurements, it is likely that the mechanism of twin wall motion is of local displacements via the motion of ledges rather than the movement of needle tips, which are relatively strongly pinned (Carpenter *et al* 2010a, Carpenter and Zhang 2011).

This simple picture of thermally activated pinning of the twin walls by defects belies more varied behaviour among different materials. For example, there appears to be no freezing interval for twin walls in $SrTiO_3$ when measurements are made at ~1–50 Hz (Schranz *et al* 1999, Kityk *et al* 2000a, 2000b, Lemanov *et al* 2002). Even at tens of MHz there is additional softening which is attributable to domain wall motion (e.g. see figure 3 of Carpenter 2007a), implying that the ferroelastic twin walls in tetragonal $SrTiO_3$ are exceptionally mobile. Furthermore, changes in their mobility appear to signal changes in local structure, such as the development of local polar domains below ~50 K (Scott *et al* 2012). In exact contradistinction to this, CST samples with the *Pnma* structure do not display anelastic losses, from which it has been deduced that the combination of two tilt systems somehow causes the twin walls to become totally immobile (Harrison *et al* 2003, Daraktchiev *et al* 2006, Walsh *et al* 2008). The same pattern of relatively mobile twin walls in the $I4/mcm$ structure and immobile twin walls in the *Pnma* structure is also observed across the $SrSnO_3$–$BaSnO_3$ and $SrZrO_3$–$SrTiO_3$ solid solutions (Daraktchiev *et al* 2006, 2007, McKnight *et al* 2009a, 2009b, Zhang *et al* 2010b), but in $BaCeO_3$ anelastic softening attributable to the twin walls persists in the stability field of the *Pnma* structure (Zhang *et al* 2010a).

From this brief summary it should be apparent that deviations from the static Landau model of elastic softening accompanying phase transitions in CST perovskites will provide information about the existence of fluctuations and the mobility of twin walls. It follows, also, that there must be possibilities for engineering the properties and dynamics of twin wall motion if the dependence on structure type and solid solution can be properly understood.

3. Experimental methods

3.1. Sample preparation

Dimensions and properties of the parallelepiped samples used in the present study are listed in table 1. CST0 is pure $CaTiO_3$, CST100 is pure $SrTiO_3$, CST80 is $(Ca_{0.2}Sr_{0.8})TiO_3$, etc. Apart from CST10 they were the same as used by Walsh *et al* (2008) and had been cut from larger pellets that had been prepared by firing pressed synthetic powders of the appropriate compositions at ~1600 °C. The CST10 pellet was prepared using the same recipe from a batch of powdered sample that had been prepared originally for the study of Carpenter *et al* (2007). Routine characterization by x-ray powder diffraction showed the presence only of single phase perovskite, with the exception of CSTO which contained a small amount of rutile. Grain sizes estimated by examination of thin slices in a polarizing microscope were ~25 μm (Walsh *et al* 2008). Estimates of porosity were based on comparisons of densities determined from the measured mass and dimensions of the parallelepipeds with theoretical densities calculated from lattice parameter data of Ball *et al* (1998).

A small, irregular fragment of single crystal $CaTiO_3$ (mass 0.0498 g), was obtained separately from a larger crystal grown by the floating zone technique with powders of $CaCO_3$ and TiO_2 (99.9% purity) as described in Guennou *et al* (2010).

3.2. Data collection

RUS spectra were collected in situ at high temperatures with each parallelepiped held lightly across its corners between two alumina rods which protruded into a resistance furnace. The equipment has been described in detail by McKnight *et al* (2008), apart from the use of Stanford electronics (Migliori and Maynard 2005). Temperature was monitored by a Pt/Rh thermocouple placed within a few mm of the sample, and a small scaling factor was applied to give an estimated accuracy of ±~1 K from comparison with the $\alpha \leftrightarrow \beta$ phase transition in quartz at 846 K. Data were collected from all the samples between room temperature and ~1350 K, with large steps (~20–40 K) during heating and generally smaller steps (~1–10 K) during cooling through the expected phase transitions. A period of 15 min was allowed for thermal equilibration at each temperature before data collection.

Low temperature spectra were collected from parallelepipeds of CST0, CST95 and CST100 in the interval ~15–295 K using a helium flow cryostat and DRS Modulus II electronics described by McKnight *et al* (2007). Large temperature

Table 1. Composition, dimensions, mass, fractional porosity, room temperature values and temperature dependence of bulk and shear moduli (corrected for porosity) of the polycrystalline samples used in this study. The number following CST indicates the % $SrTiO_3$ of the sample, e.g. CST30 is $Ca_{0.7}Sr_{0.3}TiO_3$.

Sample composition	a (mm)	b (mm)	c (mm)	Mass (g)	Density (g cm^{-3})	Fractional porosity	K (GPa)	G (GPa)	dK/dT (GPa K^{-1})	dG/dT (GPa K^{-1})
CST0	4.771	4.272	3.805	0.285	3.678	0.082	165.6(3)	104.8(1)	−0.0295(3)[a]	−0.0183(3)[a]
CST10	3.756	3.497	2.829	0.144	3.873	0.066	171.1(1)	104.9(1)	−0.0299(3)[a]	−0.0199(2)[a]
CST30	3.787	2.792	3.265	0.139	4.031	0.076	187.4(6)	104.3(1)	−0.038(3)[a]	−0.0234(5)[a]
CST50	2.802	3.252	3.273	0.145	4.259	0.069	180.1(11)	100.6(1)	−0.030(2)[b]	−0.0149(8)[b]
CST65	3.666	2.707	3.699	0.161	4.427	0.066	169.9(8)	86.4(1)	−0.0248(5)[b]	−0.0192(5)[b]
CST80	2.868	3.272	3.781	0.156	4.543	0.072	171.3(8)	87.5(1)	−0.0264(4)[b]	−0.0191(2)[b]
CST95	2.777	2.301	3.281	0.100	4.770	0.057	165.7(9)	116.9(1)	−0.0221(1)[b]	−0.0263(4)[b]
CST100	3.786	3.312	2.897	0.177	4.859	0.050	174.9(5)	117.5(1)	−0.0289(4)[b]	−0.0226(3)[b]

[a] Temperature dependence for *Pnma* structure.

[b] Temperature dependence for $Pm\bar{3}m$ structure.

steps (∼20–40 K) were used during cooling and narrower temperature steps (∼1–10 K) during heating through phase transitions. Temperature was monitored with a Si-diode and is believed to be accurate to at least ±0.5 K, as checked against the phase transition point of $SrTiO_3$. A period of 15 min was allowed for thermal equilibration before data collection at each temperature.

3.3. Data analysis

Resonance spectra obtained for each sample were loaded into the software package IGOR Pro (Wavemetrics) for analysis. Values of K and G were then determined from fitting to the measured frequencies, f, of between 10 and 30 resonance peaks using DRS software (Migliori and Sarrao 1997), with typical rms errors of ∼0.3% for the fitting. Lattice parameter data of Redfern (1996) and Carpenter *et al* (2006b) were used to estimate the effects of thermal expansion on the dimensions of the parallelepipeds and corrections for porosity were also applied, using the expressions of Ledbetter *et al* (1994). Estimates of uncertainties in the values of K and G obtained in this way, based largely on output from the DRS software, are <∼1.4% and <∼0.2%, respectively. Individual resonances of a parallelepiped are dominated by shearing, so that estimates of G can also be obtained from the frequencies of a single peak, according to

$$G_{\mathrm{calc}} = af^2, \tag{1}$$

where the value of the scaling coefficient, a, is obtained from the measured values of f and G at room temperature.

An asymmetric Lorentzian function was used to fit selected individual peaks in order to determine values of Q^{-1}, given by $Q^{-1} = \Delta f/f$, where Δf is the peak width at half maximum height.

4. Results

Figure 3 includes stacks of spectra as examples of the primary RUS data for two samples, CST30 and CST80. The y-axis is amplitude, in volts, but spectra have been offset in proportion to the temperature at which they were collected so as to visualize the changes in frequency of resonance peaks. In CST30, $Pm\bar{3}m \leftrightarrow I4/mcm$ and $I4/mcm \leftrightarrow Pnma$ transitions occur at ∼1200 and ∼970 K respectively. Sharp peaks are present in spectra collected over the entire temperature interval, apart from in the stability field of the tetragonal phase, and there is distinct softening (lowering of frequency) as the transition temperature for the $Pm\bar{3}m \leftrightarrow I4/mcm$ transition is approached from above and below. Similar softening occurs with falling temperature in CST80, but continues below the $Pm\bar{3}m \leftrightarrow I4/mcm$ transition point at ∼500 K. Figure 4 contains data for K, G, G_{calc} and Q^{-1} extracted from these spectra and equivalent spectra collected for the other samples used in this study. Transition temperatures have been added as vertical broken lines to the graphs for individual samples and are compatible with expectations from figure 1. For some samples, increases in K accompanied by significant scatter were observed close to phase transitions and in the stability field of the $I4/mcm$ structure. This is not thought to be a real effect and is most likely due to poor constraints from fitting of a small number of peaks. Linear temperature dependences for K and G (dK/dT, dG/dT) have been obtained by fitting to data for $Pm\bar{3}m$ and *Pnma* structures and are listed in table 1.

4.1. CST0

As found also by Walsh *et al* (2008), both K and G for the polycrystalline sample reduce with increasing temperature in a manner that could be accounted for by the normal effects of thermal expansion (figure 4(*a*)). A slight increase in values of Q^{-1} between ∼900 K and room temperature does not appear to correlate with any obvious change in the elastic properties. Spectra from the single crystal did not show this increase in dissipation, however, and since twin wall motion might be expected to be similar in both samples this is perhaps derived from other aspects of the microstructure. The sample contains a small proportion of impurity phase rutile, for example. Frequency data for the polycrystalline sample showed slight hysteresis between heating and cooling, suggesting that some recrystallization may have taken place at the highest temperatures.

4.2. CST10

As for CST0, the main pattern of softening with increasing temperature in the stability field of the *Pnma* structure is

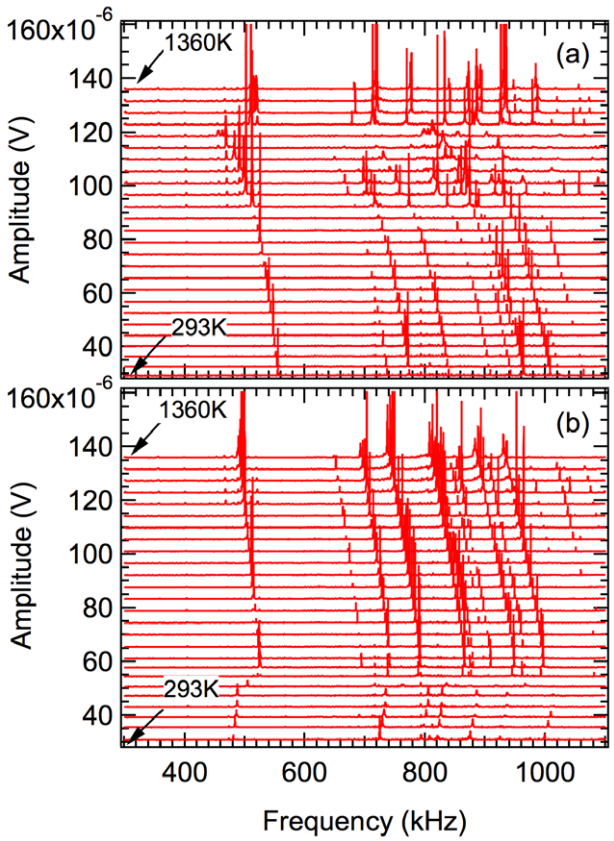

Figure 3. Selected resonance spectra obtained during cooling for CST30 (*a*) and CST80 (*b*). Each spectrum has been offset up the *y*-axis in proportion to the temperature at which it was collected. All the resonance peaks of CST30 shift to lower temperatures as the $Pm\bar{3}m \leftrightarrow I4/mcm$ and $I4/mcm \leftrightarrow Pnma$ transitions (at ∼1200 K and ∼970 K, respectively) are approached with increasing and decreasing temperature. Softening below the $Pm\bar{3}m \leftrightarrow I4/mcm$ transition (at ∼500 K) in CST80 is indicated by the shift to lower frequencies, and is accompanied by broadening of the resonance peaks.

gradual and continuous. An additional softening effect was found in G and G_{calc} as the $I4/mcm \leftrightarrow Pnma$ transition was approached. Q^{-1} remained low from room temperature up to ∼1150 K, when a slight increase is observed (figure 4(*b*)).

4.3. CST30

The stability field of the $I4/mcm$ structure of CST30 is clearly marked by higher values of Q^{-1} than are observed for either of the $Pm\bar{3}m$ or *Pnma* structures (figure 4(*c*)). There is slight softening of G as the $Pm\bar{3}m \leftrightarrow I4/mcm$ transition is approached from either side, but the transition itself is marked by an abrupt softening with falling temperature. There is also some slight softening of G as the $I4/mcm \leftrightarrow Pnma$ transition is approached, but no obvious discontinuity. Any changes in K associated with either transition are less than the noise in the data.

4.4. CST50

As found also by Walsh *et al* (2008), the stability field of the $I4/mcm$ structure in CST50 is marked by the complete absence of resonance peaks (figure 4(*d*)), corresponding to $Q^{-1} >\sim 0.02$. Q^{-1} remains low at all temperatures where spectra were collected in the stability fields of the $Pm\bar{3}m$ and *Pnma* structures. Data for CST50 from Carpenter and Zhang (2011) have been included for completeness. These were not previously corrected for temperature with respect to the quartz transition point or for the effects of thermal expansion and porosity. The same temperature correction as applied to the new data was applied, therefore, and absolute values of K and G were scaled by 1.18 and 1.135 to make them overlap with data collected for the present study.

4.5. CST65

The stability field of the $Pm\bar{3}m$ structure of CST65 is marked by slight softening of G as the $Pm\bar{3}m \leftrightarrow I4/mcm$ transition is approached from above and low Q^{-1} values at all temperatures at which spectra were collected (figure 4(*e*)). The transition itself at ∼710 K is marked by the abrupt disappearance of resonance peaks but these start to return below ∼500 K. There is then a steep reduction in Q^{-1} down to the $I4/mcm \leftrightarrow Pbcm$ transition. Within the stability field of the *Pbcm* structure, Q^{-1} returns to the low values of the $Pm\bar{3}m$ structure. There is only a small dip in G at the $I4/mcm \leftrightarrow Pbcm$ transition. Data at temperatures below 315 K have been reproduced from Manchado *et al* (2009), with appropriate correction and scaling to account for porosity.

4.6. CST80

The pattern of evolution of K, G and Q^{-1} for CST80 is essentially the same as for CST65 (figure 4(*f*)). In this case it was possible to follow the resonance peaks below the $Pm\bar{3}m \leftrightarrow I4/mcm$ transition temperature, however. The transition is marked by a steep increase in Q^{-1} and softening of G. Below the transition, G remains almost constant and there is a very slight increase in K which may be real.

4.7. CST95

In CST95 the $Pm\bar{3}m \leftrightarrow I4/mcm$ transition is expected to occur at approximately 220 K and a transition to '*mm*2' is expected to occur at approximately 35 K. Marked softening of G and an increase in Q^{-1} occur at ∼235 K, however, which clearly defines the first transition at this composition (figure 4(*g*)). In contrast with CST80, further elastic softening and increasing Q^{-1} then occurs with falling temperature below ∼220 K. Resonance peaks could not be distinguished from noise in spectra collected below ∼180 K.

4.8. CST100

Data for CST100 from McKnight *et al* (2009b) have been added to data collected in the present study and are shown in figure 4(*h*). Resonance peaks weaken with falling temperature and the lowest temperature for which values of both K and G data were obtained is 115 K, slightly above the $Pm\bar{3}m \leftrightarrow I4/mcm$ transition temperature of ∼106 K. G softens as the phase transition is approached, but little variation is seen

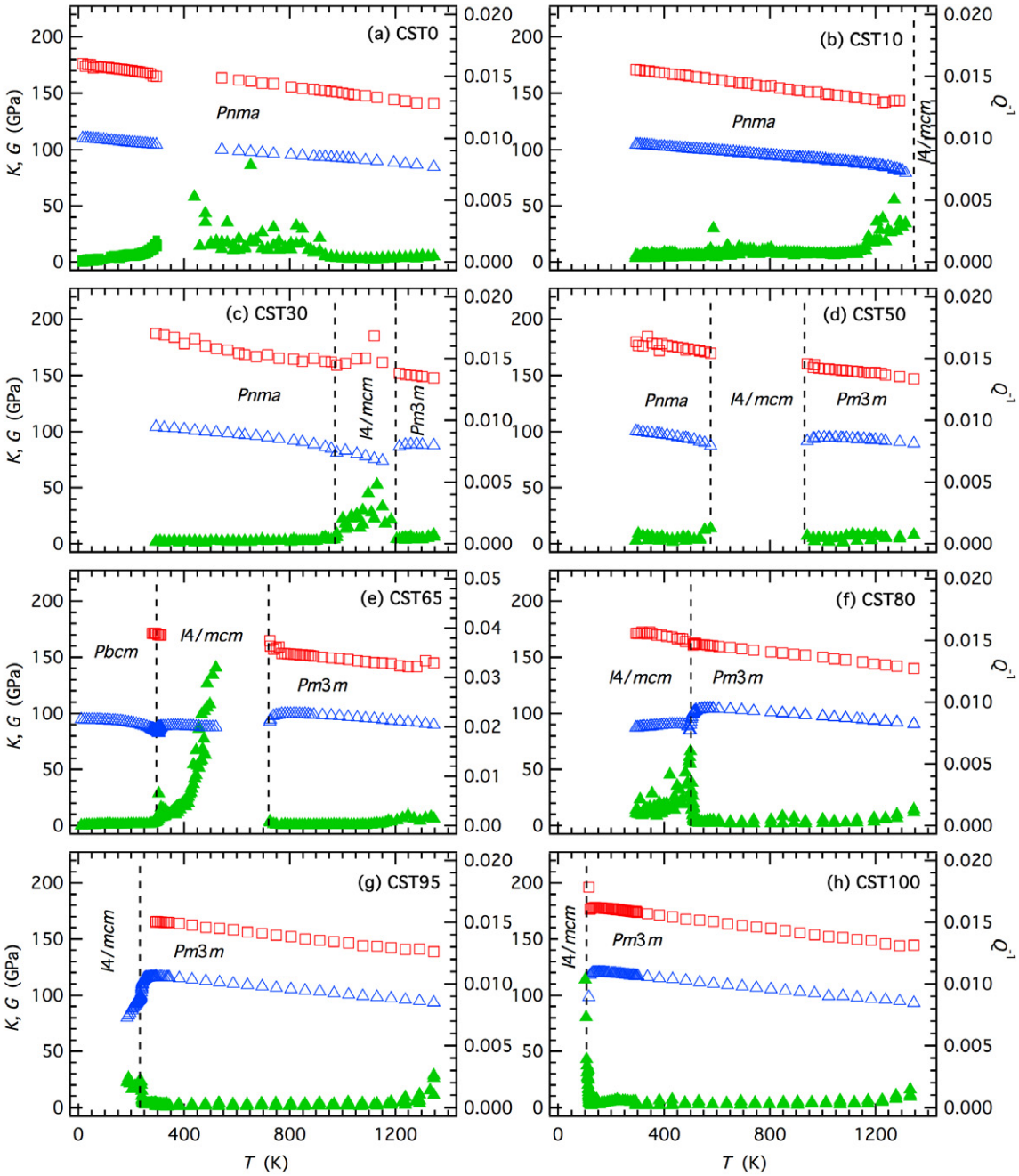

Figure 4. Data for the bulk modulus, K, (red open squares) shear modulus, G, (blue open triangles) and inverse mechanical quality factor, Q^{-1}, (green filled triangles) for polycrystalline samples of CST perovskite from RUS data. Error bars for fit values of K and G are smaller than the size of the symbols. Vertical broken lines mark the $Pm\bar{3}m \leftrightarrow I4/mcm$, $I4/mcm \leftrightarrow Pnma$ and $I4/mcm \leftrightarrow Pbcm$ transition temperatures. Selected data for CST65 from Manchado *et al* (2009) and for CST50 from Carpenter and Zhang (2011) have been included for completeness.

in Q^{-1}. There is complete attenuation of acoustic resonances below the transition temperature.

5. Discussion

The objective of the present study was to examine patterns of strain coupling, elastic softening and anelastic loss across the CST solid solution. A complete and quantitative calibration of the strain and softening behaviour was already completed for $SrTiO_3$ (Carpenter 2007a), and the expectation is that the overall behaviour across the solid solution will also conform to the precepts of Landau theory as expressed by a single master equation for the excess free energy, G_L, with respect to the cubic parent structure (after Carpenter *et al* 2001, Carpenter 2007a, McKnight *et al* 2009a):

$$G_L = \frac{1}{2}a_1\Theta_{s1}\left(\coth\left(\frac{\Theta_{s1}}{T}\right) - \coth\left(\frac{\Theta_{s1}}{T_{c1}}\right)\right)\left(q_1^2 + q_2^2 + q_3^2\right)$$
$$+\frac{1}{2}a_2\Theta_{s2}\left(\coth\left(\frac{\Theta_{s2}}{T}\right) - \coth\left(\frac{\Theta_{s2}}{T_{c2}}\right)\right)\left(q_4^2 + q_5^2 + q_6^2\right)$$

$$
\begin{aligned}
&+\frac{1}{4}b_1\left(q_1^2+q_2^2+q_3^2\right)^2+\frac{1}{4}b_1'\left(q_1^4+q_2^4+q_3^4\right)\\
&+\frac{1}{4}b_2\left(q_4^2+q_5^2+q_6^2\right)^2+\frac{1}{4}b_2'\left(q_4^4+q_5^4+q_6^4\right)\\
&+\frac{1}{6}c_1\left(q_1^2+q_2^2+q_3^2\right)^3+\frac{1}{6}c_1'\left(q_1q_2q_3\right)^2\\
&+\frac{1}{6}c_1''\left(q_1^2+q_2^2+q_3^2\right)\left(q_1^4+q_2^4+q_3^4\right)+\frac{1}{6}c_2\left(q_4^2+q_5^2+q_6^2\right)^3\\
&+\frac{1}{6}c_2'\left(q_4q_5q_6\right)^2+\frac{1}{6}c_2''\left(q_4^2+q_5^2+q_6^2\right)\left(q_4^4+q_5^4+q_6^4\right)\\
&+\lambda_{\mathrm{q}}\left(q_1^2+q_2^2+q_3^2\right)\left(q_4^2+q_5^2+q_6^2\right)\\
&+\lambda_{\mathrm{q}}'\left(q_1^2q_4^2+q_2^2q_5^2+q_3^2q_6^2\right)\\
&+\lambda_1e_{\mathrm{a}}\left(q_1^2+q_2^2+q_3^2\right)+\lambda_2e_{\mathrm{a}}\left(q_4^2+q_5^2+q_6^2\right)\\
&+\lambda_3\left[\sqrt{3}e_{\mathrm{o}}\left(q_2^2-q_3^2\right)+e_{\mathrm{t}}\left(2q_1^2-q_2^2-q_3^2\right)\right]\\
&+\lambda_4\left[\sqrt{3}e_{\mathrm{o}}\left(q_5^2-q_6^2\right)+e_{\mathrm{t}}\left(2q_4^2-q_5^2-q_6^2\right)\right]\\
&+\lambda_5\left(e_4q_4q_6+e_5q_4q_5+e_6q_5q_6\right)\\
&+\lambda_6\left(q_1^2+q_2^2+q_3^2\right)\left(e_4^2+e_5^2+e_6^2\right)\\
&+\lambda_7\left(q_1^2e_6^2+q_2^2e_4^2+q_3^2e_5^2\right)\\
&+\frac{1}{4}\left(C_{11}^{\mathrm{o}}-C_{12}^{\mathrm{o}}\right)\left(e_{\mathrm{o}}^2+e_{\mathrm{t}}^2\right)+\frac{1}{6}\left(C_{11}^{\mathrm{o}}+2C_{12}^{\mathrm{o}}\right)e_{\mathrm{a}}^2\\
&+\frac{1}{2}C_{44}^{\mathrm{o}}\left(e_4^2+e_5^2+e_6^2\right). \qquad (2)
\end{aligned}
$$

where q_1–q_3 are components of the order parameter for M-point tilting, q_4–q_6 are components of the order parameter for R-point tilting, T_c's are critical temperatures for the two critical points, Θ_s's are saturation temperatures, a, b, c..... are Landau coefficients, e_a, e_t and e_o are, respectively, volume, tetragonal shear and orthorhombic shear strains, e_4–e_6 are off-diagonal components of the spontaneous strain tensor, λ's are strain order parameter coupling coefficients and C_{ik}^{o} are elastic constants of the cubic reference structure. Variations of the elastic constants for structures with space groups which are symmetry subgroups are obtained from this using the equations of Slonczewski and Thomas (1970).

5.1. Patterns of elastic softening due to the $Pm\bar{3}m \leftrightarrow I4/mcm$ transition

All the data for K as a function of temperature at different compositions are shown together in figure 5(*a*). Apart from scatter close to the $Pm\bar{3}m \leftrightarrow I4/mcm$ transition temperatures, it is clear that any softening in the stability field of the cubic structure is small and that any softening due to the phase transitions themselves is barely greater than the experimental uncertainties. The difference in bulk modulus between the tetragonal phase, K, and the cubic phase, K^{o}, for the Voigt limit is

$$K_{\mathrm{Voigt}} = K^{\mathrm{o}} - 4\lambda_2^2R_{44}q_4^2, \qquad (3)$$

where λ_2 defines the strength of coupling between the tilt order parameter, q_4, and the volume strain, and R_{44} is the order parameter susceptibility (McKnight *et al* 2009a). The lack of any significant softening is consistent with analysis of the lattice parameter data which show coupling between the order parameters for octahedral tilting and volume strain

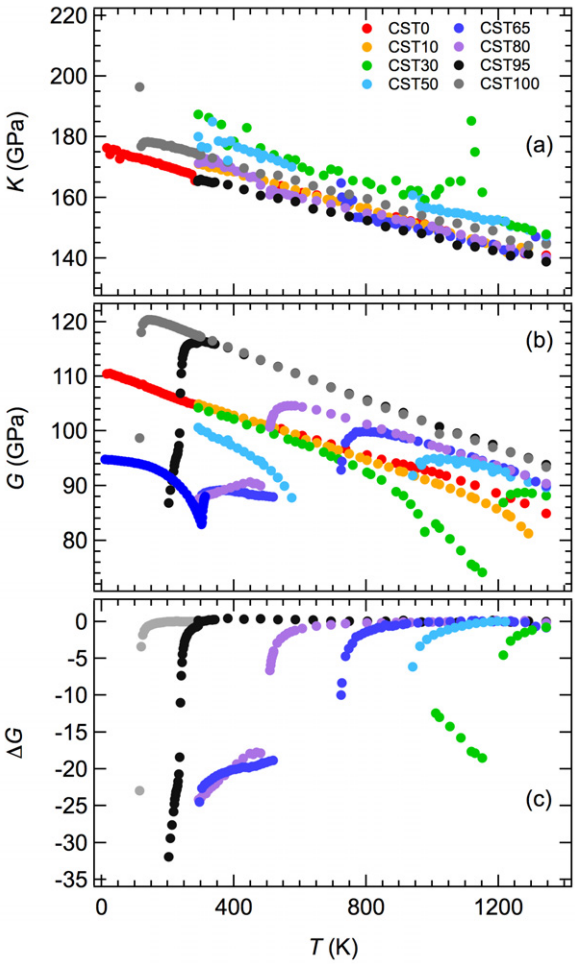

Figure 5. Summary of data for the bulk modulus and shear modulus taken from figure 4. (*a*) Bulk modulus. Apart from noisy data in the vicinity of the transition temperatures, K shows normal softening with increasing temperature and no obvious anomalies related to the tilting transitions. There is perhaps a slight additional stiffening below $T_c = \sim 500$ K for the $Pm\bar{3}m \leftrightarrow I4/mcm$ transition in CST80. (*b*) Shear modulus. There is a regular pattern of softening as a function of temperature and composition, with ~20–30% lowering of G below the $Pm\bar{3}m \leftrightarrow I4/mcm$ transition. (c) Softening of the shear modulus, ΔG, for cubic and tetragonal structures with respect to straight line fits through data for the cubic structure at temperatures away from the influence of the transition. This clearly shows precursor softening in the stability field of the cubic phase and steep softening at the $Pm\bar{3}m \leftrightarrow I4/mcm$ transition.

to be weak. In the compilation of Carpenter *et al* (2006b) values of the volume strains are smaller than ±0.001. On the other hand, the most robust data set for K (CST80) shows a very slight stiffening (best seen in figure 4(*f*)), which is presumed to be indicative of a small contribution from the next higher order term, $\lambda e_a^2q_4^2$. This form of coupling is always allowed by symmetry and will give an increase or decrease in the bulk modulus, depending on the sign of the coefficient λ, proportional to q_4^2.

Shear strains coupled to the octahedral tilting are much greater, with maximum values of up to ~0.008 for the tetragonal strain, e_t (Carpenter *et al* 2006b). This stronger coupling, derived from relatively large values of the coupling coefficients λ_4 and λ_5, is then reflected also in the marked

softening of the shear modulus, G, through the $Pm\bar{3}m \leftrightarrow I4/mcm$ transition (figure 5(b)). The influence of different parameters on the total softening below T_c is most easily seen in the expression for the shear modulus at the Voigt limit (from McKnight *et al* 2009)

$$G_{\text{Voigt}} = \frac{1}{5}\left(C_{11}^{o} - C_{12}^{o} + 3C_{44}^{o}\right) - \frac{2}{5}\left(8\lambda_4^2 R_{44} + \lambda_5^2 R_{66}\right) q_4^2, \tag{4}$$

where R_{66} is the order parameter susceptibility with respect to order parameter component q_6. The actual pattern and magnitude of softening is seen most clearly in figure 5(c), where ΔG, the difference between measured values and a straight line fit through data at temperatures well above the transition point, is shown for each composition. For CST30, G has a steep softening at T_c, followed by recovery with the expected pattern of a tricritical transition shown in figure 2(b). The size of the total step is ~20 GPa for CST30, CST65, CST80 and CST95, which is similar to the size of the same step in $SrTiO_3$ (CST100) from Carpenter (2007a), implying that the coupling coefficients in equation (4) do not vary strongly with composition across the solid solution. Carpenter (2007b) had proposed that the apparent change in thermodynamic character of the $Pm\bar{3}m \leftrightarrow I4/mcm$ transition from close to tricritical in the composition range CST0–CST90 to more nearly second order in $SrTiO_3$ could be attributed to due to changes in the values of the strain coupling coefficient, λ_4, and its influence on the value of the fourth order Landau coefficient. In the light of the constant amount of softening, this simple explanation may not be the complete picture, and the origin of the change in transition character for $SrTiO_3$ may be due more fundamentally to the dynamics of the soft mode.

By analogy with the known behaviour of $LaAlO_3$ from Brillouin scattering measurements (Carpenter *et al* 2010b), a relatively small part of the observed softening in the stability field of the tetragonal structure immediately below the transition point is likely to have come also from coupling of acoustic modes with central peak modes, related to local flipping of octahedrally tilted clusters between twin orientations.

5.2. Patterns of elastic softening due to the *I4/mcm* ↔ *Pnma* and *I4/mcm* ↔ *Pbcm* transitions

The $I4/mcm \leftrightarrow Pnma$ transition is first order in character, involving the development of M-point tilting and coupling of the new order parameter with strain. From the data for CST30 (figure 4(c)), the associated anomaly in K is small and certainly no greater than the noise in the data, consistent again with there being only weak coupling with the volume strain. Rather than there being a step in G, however, there is only a small amount of softening ahead of the transition and slight stiffening after it (figure 4(c)). As found also in $Sr(Zr,Ti)O_3$ (McKnight *et al* 2009a, 2009b), the total variation in G between the *Pnma* structure and the parent cubic structure ends up as being rather small. This is most easily understood if the total softening arises from the total strain of the *Pnma* structure with respect to the parent cubic structure, which is small, rather than as the sum of two separate strains from coupling with the individual order parameters. In particular the tetragonal shear strain, e_t, decreases in magnitude below the $I4/mcm \leftrightarrow Pnma$ transition (Carpenter *et al* 2001, McKnight *et al* 2009a). Operation of the two tilts cannot be treated in isolation, therefore, and a quantitative model of this softening would require inclusion of coupling between the M-point and R-point order parameters.

The $I4/mcm \leftrightarrow Pbcm$ transition at CST65 is marked by an anomaly in G which is also small in comparison with the anomaly at the $Pm\bar{3}m \leftrightarrow I4/mcm$ transition.

5.3. Precursor softening

At all compositions for which there are data collected in the stability field of the cubic phase, there is softening of the shear and bulk moduli as the $Pm\bar{3}m \leftrightarrow I4/mcm$ transition is approached from above, indicating the presence of local clustering or fluctuations of the octahedral tilts within an average cubic matrix. Following initial theoretical treatments (Pytte 1970, 1971, Axe and Shirane 1970, Höchli 1972) the softening is usually described at a phenomenological level using a power law of the form

$$C_{ik} - C_{ik}^{o} = \Delta C_{ik} = A_{ik}\left(T - T_c\right)^{-\kappa}. \tag{5}$$

A_{ik} is a material constant and κ is expected to take values between 1/2 and 2. This describes the softening ahead of octahedral tilting transitions in $SrTiO_3$, $LaAlO_3$ and $KMnF_3$ as well as within the stability range of the alpha phase at the $\alpha \leftrightarrow \beta$ co-elastic transition in quartz, for example (Carpenter and Salje 1998, Carpenter 2007a, Carpenter *et al* 1998, 2010a, Salje and Zhang 2009). Although derived for elastic constants which have the symmetry properties of the identity representation, i.e. the bulk modulus, it has also been applied to shear elastic constants (e.g. Carpenter *et al* 2010a, Salje and Zhang 2009).

Figure 6 is a plot of $\ln\Delta G$ versus $\ln(T - T_c)$, using T_c values of 1200 K, 719 K, 500 K, 234 K and 106 K for CST30, CST50, CST65, CST80, CST95, CST100, respectively, where ΔG is softening of the shear modulus in the stability field of the cubic phase taken from figure 5(c). The linear fits shown for three sets of data have A = 6.18, 4.33, 3.87 GPa and κ = 1.84, 1.15, 0.82 for CST100, CST95 and CST65, respectively. Values for the coefficients would be essentially indistinguishable for CST80, CST65, CST50 and CST30. In the case of elastic constants with symmetry properties related to the identity representation, $\kappa = 0.5$ would be consistent with strong dispersion of the soft mode with all three branches softening with the soft mode, and $\kappa = 1$ would be consistent with strong dispersion and flattening in two dimensions while the third remains steep (Carpenter and Salje 1998). $\kappa = 2$ would be consistent with weak dispersion in three orthogonal directions and more or less uniform softening of the each branch with the soft mode itself. On this basis the soft optic mode for most of the solid solution might conform approximately to the behaviour for $\kappa = 1$. Probably of more significance is the fact that there is a change in the exponent at the most Sr-rich compositions, implying that the properties of this soft mode are not uniform across the entire solid solution.

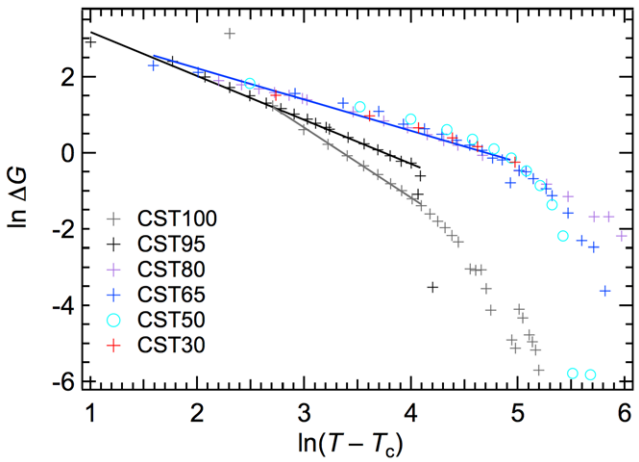

Figure 6. Softening of the shear modulus in the stability field of the cubic phase as the $Pm\bar{3}m \leftrightarrow I4/mcm$ transition is approached from above can be described by equation (5) over a reasonable temperature interval, as shown by straight lines fit to data from figure 5(*c*), plotted in ln–ln form. The three straight lines shown are fits to data for CST100, CST95 and CST65, with slopes of 1.84, 1.15, 0.82. Data for CST30, CST50 and CST80 are barely distinguishable from those for CST65.

This change in behaviour is reflected also in the steep softening with falling temperature seen even in the stability field of the tetragonal phase at CST95 and is most likely related to the proximity of the ferroelectric instability. For $LaAlO_3$, $\kappa = 1.1$ for the shear modulus (Carpenter *et al* 2010a) and for $KMnF_3$ individual shear elastic constants (C_{11}–C_{12}) and C_{44} have $\kappa = 0.5$ and 1.0 (Salje and Zhang 2009). Neither of $LaAlO_3$ and $KMnF_3$ have an additional ferroelectric instability nearby in parameter space, as far as is known.

Precursor softening in the stability field of the $I4/mcm$ structure ahead of the transitions to *Pnma* or *Pbcm* structures is also apparent in figure 5(*c*). The data for CST30 show a normal pattern of stiffening of the shear modulus with falling temperature but there is marked softening at CST65, CST80, and CST95. The steepness of the softening also increases with increasing Sr-content (figure 5(*c*)). If this was indicative of fluctuations or clustering associated specifically with the development of M-point tilting, it would be expected to occur in other perovskites with similar transition sequences, but this is not always the case. In $BaCeO_3$ there is little or no softening ahead of the transformation from the $I4/mcm$ structure to the *Imma* structure, whereas in $Sr(Zr,Ti)O_3$ some softening over a limited temperature is observed (McKnight *et al* 2009a, 2009b, Zhang *et al* 2010a, 2010b). At CST80 and CST95, there may be fluctuations or clustering as a precursor to the incipient ferroelectric transition. As mentioned in the introduction, equivalent steep softening over wide temperature intervals approaching the phase transitions of ferroelectrics or the freezing interval of ferroelectric relaxors is typical of these materials and is related also to a characteristic central peak in Brillouin scattering data.

5.4. Acoustic loss due to twin wall mobility

As found in previous studies of CST perovskites, acoustic loss behaviour provides evidence for twin wall mobility in the $I4/mcm$ structure, but in the *Pnma* structure the attenuation abruptly diminishes, signifying that the twin walls become immobile (Harrison *et al* 2003, Harrison *et al* 2003, Daraktchiev *et al* 2006, Walsh *et al* 2008, McKnight *et al* 2009a, 2009b, Zhang *et al* 2010b, Carpenter and Zhang 2011). The data presented here do not shed additional light on why the twin walls have this change in character, but they do allow some analysis of the dynamics of twin walls in the tetragonal structure as functions of both temperature and composition.

There is a characteristic pattern of dissipation associated with twin wall mobility below a ferroelastic transition point, T_c, as reproduced in figure 7(*a*) (following Harrison *et al* 2003, Harrison *et al* 2004b, Carpenter *et al* 2010a, Carpenter and Zhang 2011). The transition is marked by an increase in the loss parameter ($\tan\delta$ for a DMA experiment and Q^{-1} from RUS), followed by a plateau indicative of a regime of anelastic loss due to the mobility of twin walls through an effectively viscous medium. A Debye loss peak then marks the typical freezing interval where the walls become immobile due to pinning by defects. Below the freezing interval $\tan\delta$ and Q^{-1} revert back to values which are typically as low as in the parent para phase. As a function of temperature at constant frequency, the Debye loss peak is expected to have a form described by (from Weller *et al* 1981, Schaller *et al* 2001)

$$Q^{-1}(T) = Q_m^{-1}\left[\cosh\left\{\frac{E_a}{Rr_2(\beta)}\left(\frac{1}{T}-\frac{1}{T_m}\right)\right\}\right]^{-1}, \quad (6)$$

where Q_m^{-1} is the maximum value of the acoustic loss which occurs at temperature T_m, R is the gas constant and E_a is an activation energy. $r_2(\beta)$ is a width parameter which arises from a spread of relaxation times for the dissipation process. This expression describes loss peaks in RUS data effectively, as has been shown for the case of $Pr_{0.48}Ca_{0.52}MnO_3$ (Carpenter *et al* 2010c), for example. Effectively complete attenuation of acoustic resonances (superattenuation) in an RUS experiment usually occurs for $Q^{-1} >\sim 0.01$–0.02 unless the resonance peaks are particularly strong, so only the lower parts of the overall pattern might be observed (figure 7(*a*)).

If the dynamic properties of the twin walls are more or less independent of composition in CST, different parts of the complete loss pattern for the tetragonal phase will be sampled at different compositions because of the different temperature limits for the stability field of this structure. Segments of Q^{-1} data have been combined on this basis in figure 7(*b*). The relatively low loss plateau is seen in CST30, and the tail at low temperatures is seen in CST65. In CST50, superattenuation occurs across the entire stability field of the $I4/mcm$ phase (~575–~930 K). The pattern from figure 7(*a*) has been superimposed on figure 7(*b*), with the Debye peak shown having values of $Q_m^{-1} = 0.063$, $T_m = 570$ K and $E_a/Rr_2(\beta) = 5000$ K, to provide a plausible, if not well constrained, description of the loss behaviour.

The peak temperature, T_m, occurs when the angular measuring frequency, ω, and the relaxation time for the defects, τ, are related by $\omega\tau = 1$. The angular frequency is related to the frequency, f, of the applied stress as $\omega = 2\pi f$.

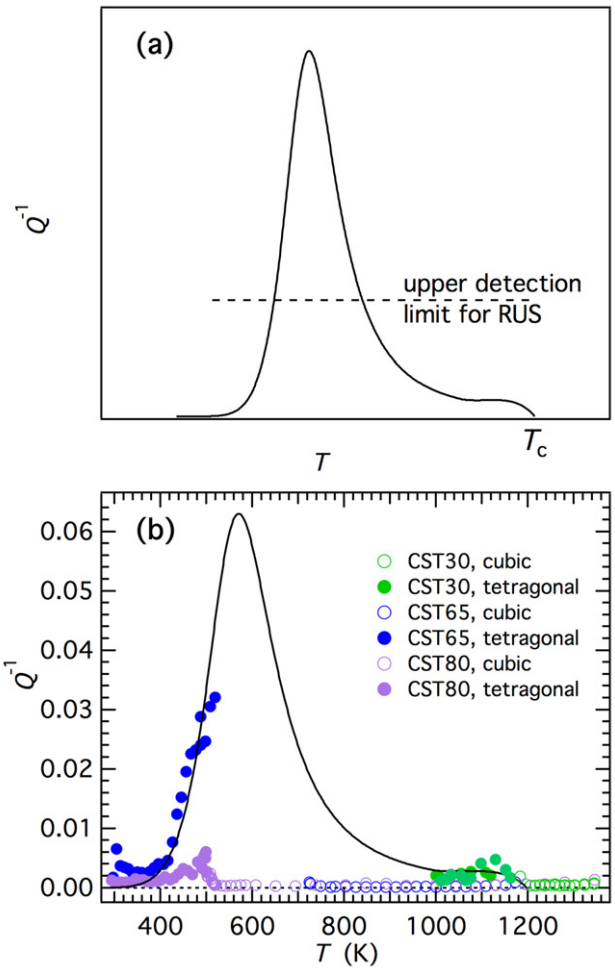

Figure 7. Characteristic patterns of acoustic dissipation for twin wall freezing in a ferroelastic material, as expressed by the variation of Q^{-1} at RUS frequencies. (*a*) Below T_c there is a plateau in Q^{-1} marking a temperature interval within which the twin walls are mobile through an effectively viscous medium. A Debye peak at lower temperatures, with a peak at $\omega\tau = 1$, then marks the freezing interval. At temperatures above the horizontal dashed line, resonance peaks become too weak to be observed by RUS (superattenuation). (*b*) By combining data for Q^{-1} in the stability field of the tetragonal phase in CST30, CST65 and CST80 it is possible to estimate the location of the curve from (*a*). The plateau region is shown as extending up to $T_c = 1200$ K for CST30 and the Debye peak shown is given by equation (6) with $Q_m^{-1} = 0.063$, $T_m = 570$ K and $E_a/Rr_2\,(\beta) = 5000$ K.

For thermally activated pinning and depinning, τ might be expected to vary in an Arrhenius manner as

$$\tau = \tau_o \exp\left(\frac{E_a}{RT}\right), \tag{7}$$

where τ_o is a constant related to the attempt frequency. Values of E_a and τ_o obtained from DMA experiments for different polycrystalline samples of CST are 96 kJ mole^{-1} and 8×10^{-14} s, 103 kJ mol^{-1} and 5×10^{-15} s (Harrison *et al* 2003), and 106 kJ mol^{-1} and 10^{-14} s (Daraktchiev *et al* 2006). Using the first set of values from Harrison *et al* (2003) and a resonance frequency of 0.5 MHz would give $\omega\tau = 1$ at ~760 K. This is not impossible but appears to be somewhat higher than the data in figure 7(*b*) imply, and the most likely explanation relates to different loss mechanisms for mobile twin walls in DMA and RUS experiments.

At the relatively high levels of applied stress in a DMA experiment, the dominant twin motion is via the back and fore displacement of the tips of needle twins, but this requires a critical stress to be exceeded for the needle tips to become unpinned (Harrison *et al* 2004a, 2004b). At the lower stresses of an RUS experiment, it is much less likely that this critical stress will be achieved and the predominant motion of twin walls is probably facilitated by lateral motion of kinks or ledges within the twin walls (Carpenter *et al* 2010a, Carpenter and Zhang 2011). This mechanism has been simulated in computer models of domain wall motion (Salje *et al* 2011, Salje *et al* 2013b). As found also for $LaAlO_3$ (Carpenter *et al* 2010a) and $KMnF_3$ (Carpenter *et al* 2012b), the value of T_m for the Debye loss peak attributed to this local mechanism of twin wall motion falls below that of the value expected by extrapolation of data collected at low frequencies by DMA, implying that the relaxation of ledges would be faster (smaller τ) than for needle tips at a given temperature. It is thus beginning to appear that this is a general result for perovskites and perhaps for ferroelastic materials more widely. There is a subtle difference also in the nature of the trends for acoustic loss immediately at T_c and below. The pattern from DMA measurements has the increase below T_c, as shown in figure 7(*a*), whereas the actual pattern for CST80 in the RUS data is of a sharp peak at or very close to T_c (figures 4(*f*) and 7(*b*)). The same peak is seen also in $Sr(Zr,Ti)O_3$ (McKnight *et al* 2009a, 2009b) and $KMnF_3$ (Carpenter *et al* 2012b). However, it is possible that this difference is intrinsic and due to an additional contribution from critical slowing down which would be detected at ~1 MHz but not at ~1 Hz.

The well-known strong acoustic attenuation at both DMA and RUS frequencies which is attributed to twin wall mobility in tetragonal $SrTiO_3$ (Schranz *et al* 1999, Kityk *et al* 2000a, 2000b, Lemanov *et al* 2002, Migliori *et al* 1993, Scott *et al* 2011) falls substantially below the characteristic freezing interval of CST perovskites. The other difference is the low transition temperature and this may account for the difference in behaviour. If the transition temperature occurs below the temperature at which point defects become immobile, there is no possibility for the defects to become concentrated on the walls and provide effective pinning. The twin walls in $SrTiO_3$ are also affected by incipient ferroelectric clusters, however, and the full richness of their structure and dynamical behaviour is still being explored (e.g. Scott *et al* 2012, Salje *et al* 2013c, Erba *et al* 2013).

The mobile twin walls of tetragonal CST are in stark contrast with the apparently immobile twin walls of the orthorhombic structure, with the same difference seen also in $Sr(Zr,Ti)O_3$ perovskites (McKnight *et al* 2009a, 2009b, Zhang *et al* 2010b). The *Pnma* phase of $BaCeO_3$ shows acoustic loss at RUS frequencies, however, so it is not clear that the difference is fundamental to systems with two tilt systems as opposed to only one (Zhang *et al* 2010a).

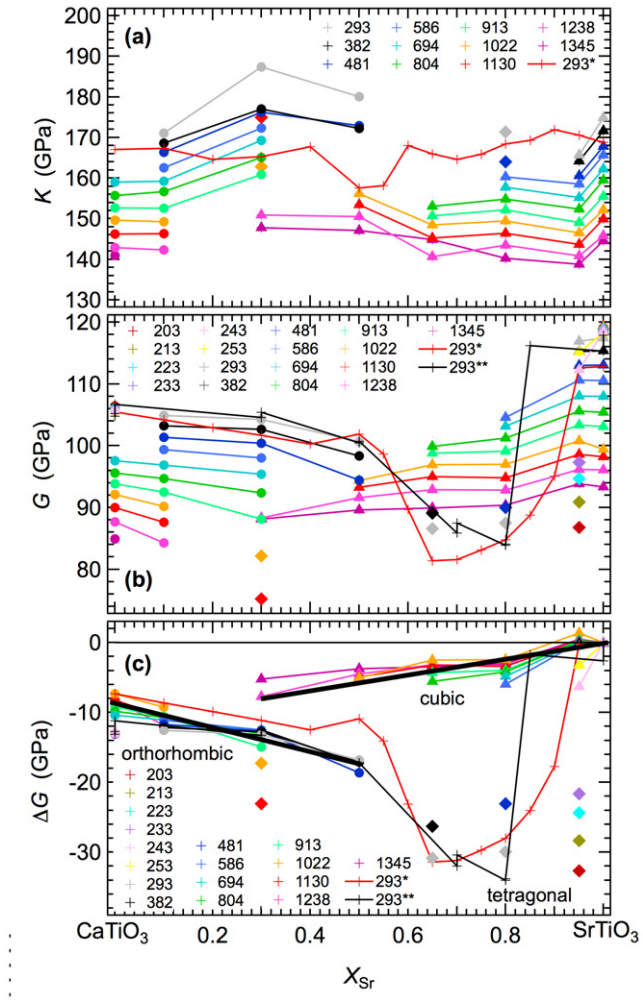

Figure 8. Data for K and G as a function of composition at different temperatures across the CST solid solution. Numbers are temperature in K. Single asterisk indicates room temperature values from Carpenter *et al* 2007; double asterisk indicates data from Walsh *et al* (2008). Triangles = cubic, diamonds = tetragonal, circles = orthorhombic. (*a*) Values of the bulk modulus do not vary greatly with composition. (*b*) Substantial variations of the shear modulus correlate essentially with stability fields of cubic, tetragonal and orthorhombic structures. (*c*) Variations of ΔG (from figures 5(*b*) and (*c*)) show well defined trends for the three main structure types and there are differences in shear modulus values of up to ~25% between them.

5.5. Composition-dependence of elastic properties

There are few, if any, solid solutions for which such a comprehensive data set of bulk and shear modulus values has been obtained as a function of both temperature and composition. The temperature dependences are seen clearly in figures 4 and 5, and the data have been plotted differently in figure 8 to show the corresponding composition dependences. The bulk modulus is at most only weakly influenced by the phase transitions, but the *Pnma* structure perhaps has a larger temperature dependence than either of the $Pm\bar{3}m$ or $I4/mcm$ structures (figure 8(*a*)). On the other hand, the marked anomalies in G due to the transitions produced variations with composition of up to ~30% which correlate with the stability fields of the different structure types in figure 1 (figures 8(*b*) and (*c*)).

At room temperature, the cubic structure is stiffest with respect to shear, the tetragonal structure is softest and the orthorhombic structure is intermediate between these (figure 8(*b*)). This is the same as reported previously by Walsh *et al* (2008) and the absolute values, including corrections to allow for porosity, are in close agreement with values obtained by pulse-echo ultrasonics at 40 MHz (data of Carpenter *et al* 2007 in figure 3 of Walsh *et al* 2008). The same pattern extends to high temperatures (figure 8(*b*)) and by considering only the softening with respect to the cubic parent structure, ΔG, it is clear that this is determined effectively by the influence of the phase transitions alone (figure 8(*c*)). Softening in the cubic phase with increasing Ca-content away from $SrTiO_3$ and in the *Pnma* phase with increasing Sr-content away from $CaTiO_3$ appears to be due to precursor effects ahead of transitions to the tetragonal phase.

A generally similar pattern of softening has been observed across the $SrZrO_3$–$SrTiO_3$ (SZT) solid solution (McKnight *et al* 2009a, 2009b). The pattern of phase transitions is closely similar, apart from the stability field for the *Imma* structure in SZT and for the *Pbcm* structure in CST. The magnitudes of the shear strains in $SrZrO_3$ are less than those in $CaTiO_3$, however, with the values of e_4 at room temperature near 0.004 in the former and ~ near 0.011 in the latter (Carpenter *et al* 2001, McKnight *et al* 2009a). The difference must extend across the two solid solutions and is reflected in lower acoustic losses associated with twin wall motion in SZT. The magnitudes of the changes in shear modulus are rather similar, however, reflecting the contribution of the soft mode itself as well as of the strain coupling coefficients in determining the intrinsic softening behaviour. In both solid solutions there is a marked increase in the steepness of softening with falling temperature of the tetragonal structure as the end member $SrTiO_3$ composition is approached (compare figure 6 of McKnight *et al* 2009b with figure 4 of this study). This further emphasizes the rather special characteristics of $SrTiO_3$ and, in particular, its proximity to a ferroelectric instability.

6. Conclusion

Strain/order parameter coupling is not unique to octahedral tilting in perovskite solid solutions and comparable ranges of elastic properties must also occur across solid solutions which undergo other types of phase transitions. In (La,Pr)AlO_3, for example, there is an additional electronic (Jahn–Teller) instability which contributes a substantial shear strain and, hence, to large softening of the shear modulus and a substantial difference in the low temperature evolution of the shear modulus with composition because Pr^{3+} is Jahn–Teller active while La^{3+} is not (Thomson *et al* 2010). There is a long tradition of choosing end-member phases of perovskites with specific combinations of phase transitions in order to produce functional materials in which properties are optimized in the solid solution, such as for piezoelectric properties in $PbTiO_3$–$PbZrO_3$. Manganite solid solutions such as $LaMnO_3$–$CaMnO_3$, $LaMnO_3$–$SrMnO_3$ and $PrMnO_3$–$CaMnO_3$ have a great diversity of magnetic and electrical properties (Salamon and Jaime 2001, Chatterji 2004), and the trend is to produce

more complex ternary (or higher order) solid solutions, such as $Pb(In_{1/2}Nb_{1/2})O_3$–$Pb(Mg_{1/3}Nb_{2/3})O_3$–$PbTiO_3$ for ferroelectric relaxor properties (Zhang and Li 2012) or $Pb(Fe_{1/2}Ta_{1/2})O_3$–$PbZrO_3$–$PbTiO_3$ for multiferroics (Evans *et al* 2013). While tailoring the elastic properties of these is rarely the primary objective, strain relaxation and strain coupling with multiple order parameters form an essential part of the physics of their underlying transformation behaviour. As a consequence, their elastic and anelastic properties will show wide variations which can be diagnostic of their particular transformation mechanisms and microstructure dynamics.

For the particular case of $CaTiO_3$–$SrTiO_3$, substantial softening of the shear modulus occurs as an intrinsic part of the cubic ↔ tetragonal phase transition. On the other hand, the tetragonal ↔ orthorhombic transition is accompanied by stiffening of the shear modulus, which has been interpreted as being due to the operation of the two tilt systems which are strongly coupled rather than completely separate instabilities. This difference in intrinsic properties is also reflected in substantially different anelastic behaviour due to twin walls being mobile in the tetragonal phase and immobile in the orthorhombic phase. Precursor softening effects across the entire solid solution can be understood simply in terms of the influence of fluctuations related to the soft optic mode on the acoustic modes. Because of the unique characteristics of $SrTiO_3$ in relation to the influence of an incipient ferroelectric transition, however, the Sr-rich members of the solid solution also show additional softening effects which may be indicative of more relaxor-like characteristics due to local ferroelectric clustering.

Acknowledgments

The RUS facilities in Cambridge were established with support from the Natural Environment Research Council (grant nos. NER/A/S/2000/01055 and NE/F017081/1), which is gratefully acknowledged. Mael Guennou is thanked for providing the single crystal of $CaTiO_3$.

References

Ali R and Yashima M 2005 *J. Solid State Chem.* **178** 2867–72
Aktas O, Salje E K H, Crossley S, Lampronti G I, Whatmore R W, Mathur N D and Carpenter M A 2013 *Phys. Rev.* B **88** 174112
Axe J D and Shirane G 1970 *Phys. Rev.* B **1** 342–8
Ball C J, Begg B D, Cookson D J, Thorogood G J and Vance E R 1998 *J. Solid State Chem.* **139** 238–47
Bednorz J G and Müller K A 1984 *Phys. Rev. Lett.* **52** 2289–92
Bianchi U, Kleemann W and Bednorz J G 1994a *Ferroelectrics* **157** 165–70
Bianchi U, Kleemann W and Bednorz J G 1994b *J. Phys.: Condens. Matter* **6** 1229–38
Bianchi U, Dec J, Kleemann W and Bednorz J G 1995 *Phys. Rev.* B **51** 8737–46
Carpenter M A and Salje E K H 1998 *Eur. J. Mineral.* **10** 693–812
Carpenter M A, Salje E K H, Graeme-Barber A, Wruck B, Dove M T and Knight K S 1998 *Am. Mineral.* **83** 2–22
Carpenter M A, Becerro A I and Seifert F 2001 *Am. Mineral.* **86** 348–63
Carpenter M A, Sondergeld P, Li B, Liebermann R C, Walsh J W, Schreuer J and Darling T W 2006 *J. Mineral. Petrol. Sci.* **101** 95–109
Carpenter M A, Howard C J, Knight K S and Zhang Z 2006b *J. Phys.: Condens. Matter* **18** 10725–49
Carpenter M A 2006 *Am. Mineral.* **91** 229–46
Carpenter M A 2007a *Am. Mineral.* **92** 309–27
Carpenter M A 2007b *Am. Mineral.* **92** 328–43
Carpenter M A, Li B and Liebermann R C 2007 *Am. Mineral.* **92** 344–55
Carpenter M A 2009 *Am. Mineral.* **94** 1084
Carpenter M A, Buckley A, Taylor P A and Darling T W 2010a *J. Phys.: Condens. Matter* **22** 035405
Carpenter M A, Sinogeikin S V and Bass J D 2010b *J. Phys.: Condens. Matter* **22** 035404
Carpenter M A, Howard C J, McKnight R E A, Migliori A, Betts J B and Fanelli V R 2010c *Phys. Rev.* B **82** 134123
Carpenter M A and Zhang Z 2011 *Geophys. J. Int.* **186** 279–95
Carpenter M A, Bryson J F J, Catalan G, Zhang S J and Donnelly N J 2012a *J. Phys.: Condens. Matter* **24** 045902
Carpenter M A. Salje E K H and Howard C J 2012b *Phys. Rev.* B **85** 224430
Chatterji T 2004 *Colossal Magnetoresistive Manganites* (Dordrecht: Kluwer)
Cowley R A, Buyers W J L and Dolling G 1969 *Solid State Commun.* **7** 181–84
Cummins H Z 1979 *Phil. Trans. R. Soc. Lond.* A **293** 393–405
Daraktchiev M, Harrison R J, Mountstevens E H and Redfern S A T 2006 *Mater. Sci. Eng.* A **442** 199–203
Daraktchiev M, Salje E K H, Lee W T and Redfern S A T 2007 *Phys. Rev.* B **75** 134102
Erba A, El-Kelany Kh E, Ferrero M, Baraille I and Rérat M 2013 *Phys. Rev.* B **88** 035102
Evans D M, Schilling A, Kumar A, Sanchez D, Ortega N, Arredondo M, Katiyar R S, Gregg J M and Scott J F 2013 *Nature Commun.* **4** 1534
Farnsworth S M, Kisi, E H and Carpenter M A 2011 *Phys. Rev.* B **84** 174124
Fossheim K and Berre B 1972 *Phys. Rev.* B **5** 3292–308
Fossum J O 1985 *J. Phys. C: Solid State Phys.* **18** 5531–48
Guennou M, Bouvier P, Krikler B, Kreisel J, Haumont R and Garbarino G 2010 *Phys. Rev.* B **82** 134101
Harrison R J and Redfern S A T 2002 *Phys. Earth Planet. Int.* **134** 253–72
Harrison R J, Redfern S A T and Street J 2003 *Am. Mineral.* **88** 574–82
Harrison R J, Redfern S A T and Salje E K H 2004a *Phys. Rev.* B **69** 144101
Harrison R J, Redfern S A T, Buckley A and Salje E K H 2004b *J. Appl. Phys.* **95** 1706–17
Hayward S A and Salje E K H 1999 *Phase Transit.* **68** 501–22
Höchli U T 1972 *Phys. Rev.* B **6** 1814–23
Howard C J, Knight K S, Kennedy B J and Kisi E H 2000 *J. Phys.: Condens. Matter* **12** L677–83
Howard C J, Withers R L, Knight K S and Zhang Z 2008 *J. Phys.: Condens. Matter* **20** 135202
Itoh M, Wang R, Inaguma Y, Yamaguchi T, Shan Y-J and Nakamura T 1999 *Phys. Rev. Lett.* **82** 3540–3
Itoh M and Wang R 2000 *Appl. Phys. Lett.* **76** 221–3
Itoh M and Wang R 2003 *J. Phys. Soc. Japan* **72** 1310–1
Itoh M, Yagi T, Uesu Y, Kleeman W and Blinc R 2004 *Sci. Technol. Adv. Mater.* **5** 417–24
Kennedy B J, Howard C J and Chakoumakos B C 1999 *J. Phys.: Condens. Matter* **11** 1479–88
Kim T H, Kojima S and Ko J-H 2012 *J. Appl. Phys.* **111** 054103
Kityk A V, Schranz W, Sondergeld P, Havlik D, Salje E K H and Scott J F 2000a *Phys. Rev.* B **61** 946–56
Kityk A V, Schranz W, Sondergeld P, Havlik D, Salje E K H and Scott J F 2000b *Europhys. Lett.* **50** 41–7
Kleemann W, Bianchi U, Bürgel A, Prasse M and Dec J 1995 *Phase Transit.* **55** 57–68

Kleemann W, Albertini A, Kuss M and Lindner R 1997 *Ferroelectrics* **203** 57–64
Ko J-H, Kim D H, Kojima S, Chen W and Ye Z-G 2006 *J. Appl. Phys.* **100** 066106
Ko J-H, Kojima S, Koo T-Y, Jung J H, Won C J and Hur N J 2008 *Appl. Phys. Lett.* **93** 102905
Laubereau A and Zurek R 1970 *Z. Naturf.* a **25** 391–401
Ledbetter H, Lei M, Hermann A and Sheng Z 1994 *Physica* C **225** 397–403
Lemanov V V, Gridnev S A and Ukhin E V 2002 *Phys. Solid State* **44** 1156–65
Lüthi B and Moran T J 1970 *Phys. Rev.* B **2** 1211–4
Lüthi B and Rehwald W 1981 *Top. Curr. Phys.* **23** 131–84
Manchado J, Romero F J, Gallardo M C, del Cerro J, Darling T W, Taylor P A, Buckley A and Carpenter M A 2009 *J. Phys.: Condens. Matter* **21** 295903
McKnight R E A, Carpenter M A, Darling T W, Buckley A and Taylor P A 2007 *Am. Mineral.* **92** 1665–72
McKnight R E A, Moxon T, Buckley A, Taylor P A, Darling T W and Carpenter M A 2008 *J. Phys.: Condens. Matter* **20** 075229
McKnight R E A, Howard C J and Carpenter M A 2009a *J. Phys.: Condens. Matter* **21** 015901
McKnight R E A, Kennedy B J, Zhou Q and Carpenter M A 2009b *J. Phys.: Condens. Matter* **21** 015902
Migliori A, Sarrao J L, Visscher W M, Bell T M, Lei M, Fisk Z and Leisure R G 1993 *Physica* B **183** 1–24
Migliori A and Sarrao J L 1997 *Resonant Ultrasound Spectroscopy: Applications to Physics, Materials Measurements and Nondestructive Evaluation* (New York: Wiley)
Migliori A and Maynard J D 2005 *Rev. Sci. Instrum.* **76** 121301
Mishra S K, Ranjan R, Pandey D and Kennedy B J 2002 *J. Appl. Phys.* **91** 4447–52
Mishra S K, Ranjan R, Pandey D, Ranson P, Ouillon R, Pinan-Lucarre J-P and Pruzan Ph 2006 *J. Phys.: Condens. Matter* **18** 1899–912
Mitsui T and Westphal W B 1961 *Phys. Rev.* **124** 1354–9
Müller K A and Berlinger W 1971 *Phys. Rev. Lett.* **26** 13–6
Nataf G F, Li Q, Liu Y, Withers R L, Driver S L and Carpenter M A 2013 *J. Appl. Phys.* **113** 124102
Okai B and Yoshimoto J 1975 *J. Phys. Soc. Japan* **39** 162–5
Pytte E 1970 *Phys. Rev.* B **1** 924–30
Pytte E 1971 *Structural Phase Transitions and Soft Modes* (*NATO ASI*) ed E J Samuelsen *et al* (Norway, Oslo: Scandinavian University Books) pp 151–69
Qin S, Becerro A I, Seifert F, Gottsmann J and Jiang J 2000 *J. Mater. Chem.* **10** 1609–15
Qin S, Wu X, Seifert F and Becerro A I 2002 *J. Chem. Soc., Dalton Trans.* **2002** 3751–5
Ranjan R, Pandey D and Lalla N P 2000 *Phys. Rev. Lett.* **84** 3726–9
Ranjan R, Pandey D, Schuddinck W, Richard O, De Meulenaere P, Van Landuyt J and Van Tendeloo G 2001 *J. Solid State Chem.* **162** 20–8
Redfern S A T 1996 *J. Phys.: Condens. Matter* **8** 8267–75
Rehwald W 1970a *Solid State Commun.* **8** 607–11
Rehwald W 1970b *Solid State Commun.* **8** 1483–5
Rehwald W 1973 *Adv. Phys.* **22** 721–55
Ringwood A E, Kesson S E, Reeve K D, Levins D M and Ramm E J 1988 Synroc *Radioactive Waste Forms for the Future* ed W Lutze and R C Ewing (Amsterdam: North Holland) pp 233–334
Salamon M B and Jaime M 2001 *Rev. Mod. Phys.* **73** 583–628
Salje E K H, Gallardo M C, Jiménez J, Romero F J and del Cerro J 1998 *J. Phys.: Condens. Matter* **10** 5535–43
Salje E K H and Zhang H 2009 *J. Phys.: Condens. Matter* **21**, 035901
Salje E K H, Ding X, Zhao Z, Lookman T and Saxena A 2011 *Phys. Rev.* B **83** 104109
Salje E K H, Carpenter M A, Nataf G F, Picht G, Webber K, Weerasinghe J, Lisenkov S and Bellaiche L 2013a *Phys. Rev.* B **87** 014106
Salje E K H, Zhao Z, Ding X and Sun J 2013b *Am. Mineral.* **98** 1449–58
Salje E K H, Aktas O, Carpenter M A and Scott J F 2013c *Phys. Rev. Lett.* **111** 247603
Schaller R, Fantozzi G and Gremaud G 2001 *Mechanical Spectroscopy* Q^{-1}*2001: With Applications to Materials Science* (Clausthal: Trans Tech. Publ.)
Schranz W, Sondergeld P, Kityk A V and Salje E K H 1999 *Phase Transit.* **69** 61–76
Scott J F, Bryson J, Carpenter M A, Herrero-Albillos J and Itoh M 2011 *Phys. Rev. Lett.* **106** 105502
Scott J F, Salje E K H and Carpenter M A 2012 *Phys. Rev. Lett.* **109** 187601
Shirane G and Yamada Y 1969 *Phys. Rev.* **177** 858–63
Slonczewski J C and Thomas H 1970 *Phys. Rev.* B **1** 3599–608
Thomson R I, Rawson J M, Howard C J, Turczynski S, Pawlak D A, Lukasiewicz T and Carpenter M A 2010 *Phys. Rev.* B **82** 214111
Unoki H and Sakudo T 1967 *J. Phys. Soc. Japan* **23** 546–52
Walsh J N, Taylor P A, Buckley A, Darling T W, Schreuer J and Carpenter M A 2008 *Phys. Earth Planet. Int.* **167** 110–7
Webb S, Jackson I and Fitz Gerald J 1999 *Phys. Earth Planet. Int.* **115** 259–91
Weller M, Li G TY, Zhang J X, Ke T S and Diehl J 1981 *Acta Metall.* **29** 1047–54
Worlock J M, Scott J F and Fleury P A 1969 *Light Scattering of Solids* ed G B Wright (New York: Springer) pp 689–96
Yao W, Cummins H Z and Bruce R H 1981 *Phys. Rev.* B **24** 424–44
Zhang S and Li F 2012 *J. Appl. Phys.* **111** 031301
Zhang Z, Koppensteiner J, Schranz W, Betts J B, Migliori A and Carpenter M A 2010a *Phys. Rev.* B **82** 014113
Zhang Z, Koppensteiner J, Schranz W and Carpenter M A 2010b *J. Phys.: Condens. Matter* **22** 295401